



Cite this: *Dalton Trans.*, 2024, **53**,
7536

Spectroscopic and thermodynamic characterization of a cobalt-verdazyl valence tautomeric system. influence of crystal structure, solvent and counterion†

David J. R. Brook, *^a Jeffrey DaRos,^a Aamani Ponnekanti,^a Stefano Agrestini ^b and Eric Pellegrin^b

Crystallization of the verdazyl-based valence tautomeric ion $[\text{Co}(\text{dipyvd})_2]^{2+}$ (where **dipyvd** is the radical ligand 1-isopropyl-3,5-di(2'-pyridyl)-6-oxoverdazyl) with a variety of different counterions results in materials that show varying degrees of valence tautomeric (VT) transition in the solid state. The X-ray structure of the SbF_6 salt at 150 K reveals a localized structure for the $S = 1/2$ tautomer, with a Co^{3+} cation and distinct anionic and radical ligands. Comparison with the structure of the same material at 300 K reveals large structural changes in the ligand as a result of the valence tautomeric equilibrium. Data for the $S = 3/2$ form is less conclusive; X-ray spectroscopy on the PF_6 salt suggests a degree of low spin Co^{2+} character for the $S = 3/2$ tautomer at very low temperature though this is inconsistent with EPR data at similar temperatures and structural information at 150 K. Magnetic measurements on the $[\text{BAr}^F_4]^-$ and triflate salts in organic solvents show that the VT equilibrium is dependent on solvent and ion pairing effects.

Received 16th February 2024,
Accepted 1st April 2024

DOI: 10.1039/d4dt00465e

rsc.li/dalton

Introduction

Valence tautomeric (VT) compounds (compounds that switch between states that have a different electronic distribution) are interesting for their complex electronic structure as well as their possible applications.^{1–3} Fundamentally, VT compounds are asymmetric mixed valence systems; the small energy difference between tautomers results in an electronic structure that can be critically dependent on small environmental changes, and the coupling of molecular geometry with electron transfer results in an energy barrier for the tautomeric interconversion. This coupling also means that for VT systems the Born-Oppenheimer approximation may no longer be valid, and vibronic coupling must be included in a theoretical description.^{4,5}

The combination of an energy barrier and environmental sensitivity also means that VT systems have the potential for

bistability. Under particular conditions a bistable sample may exist in one of two (or more) forms that interconvert only slowly; the particular form observed depends not only on the current conditions but the history of the sample. As a result, these systems have possible application as molecular sensors, in information storage, and molecular and quantum computing.

Understanding the barrier in metal–ligand VT systems requires understanding the geometry changes occurring at both ligand and metal sites. The majority of reported valence tautomers involve a cobalt ion coordinated to an oxolene (catecholate/semiquinone/quinone) ligand system.² In many of these cases, electron transfer also results in spin crossover at the metal ion, though for some recent examples the two processes are separate.^{6–8} Spin crossover at the metal ion results in relatively large changes in bond length but changes in the ligand geometry are relatively small. Recent studies have explored other ligand systems in order to better control valence tautomerization and related geometry changes.⁹ In particular we recently reported a cobalt-verdazyl system, cobalt bis(1-isopropyl,3,5-di-(2'-pyridyl)-6-oxoverdazyl), $[\text{Co}(\text{dipyvd})_2]^{2+}$ that showed valence tautomerism between doublet and quartet states in solution, but in the solid state (as the PF_6^- salt) it was trapped as the quartet (Scheme 1).¹⁰

Studies on related species indicate the oxidized form of the ligand (a verdazyl radical) is essentially rigid and planar, however reduction by a single electron gives an antiaromatic

^aDepartment of Chemistry, San Jose State University, San Jose, CA 95192, USA.
E-mail: david.brook@sjsu.edu

^bALBA Synchrotron Light Source, E-08290 Cerdanyola del Vallès, Barcelona, Spain

† Electronic supplementary information (ESI) available: Plot of magnetization vs. applied field between 2 and 5 K for $[\text{Co}(\text{dipyvd})_2](\text{PF}_6)_2$, XAS spectrum of $[\text{Co}(\text{dipyvd})_2](\text{PF}_6)_2$ recorded at 2 K. Full details of the structure determinations of $[\text{Co}(\text{dipyvd})_2](\text{SbF}_6)_2$ and $[\text{Co}(\text{dipyvd})_2](\text{BF}_4)_2$. CCDC 2332770, 2332798, 2332805 and 2332825. For ESI and crystallographic data in CIF or other electronic format see DOI: <https://doi.org/10.1039/d4dt00465e>



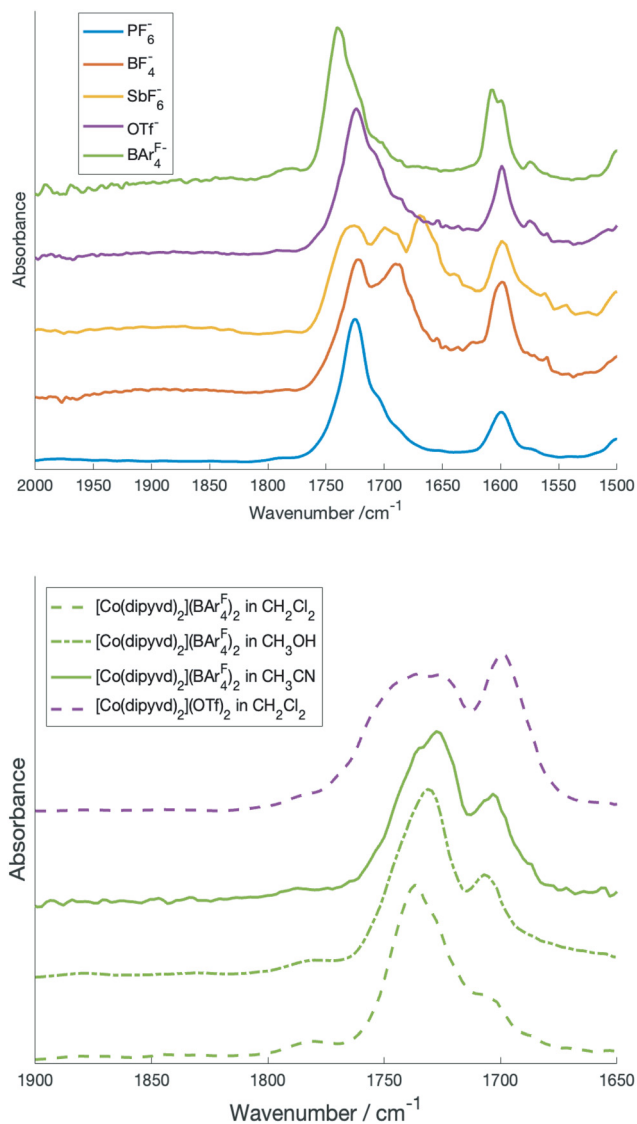


Fig. 1 Top: carbonyl region of the IR spectrum of crystalline $[\text{Co}(\text{dipyvd})_2]^{2+}$ salts. Bottom: carbonyl region of $[\text{Co}(\text{dipyvd})_2]^{2+}(\text{BARF}_4^-)_2$ and $[\text{Co}(\text{dipyvd})_2]^{2+}(\text{OTf})_2$ in solution.

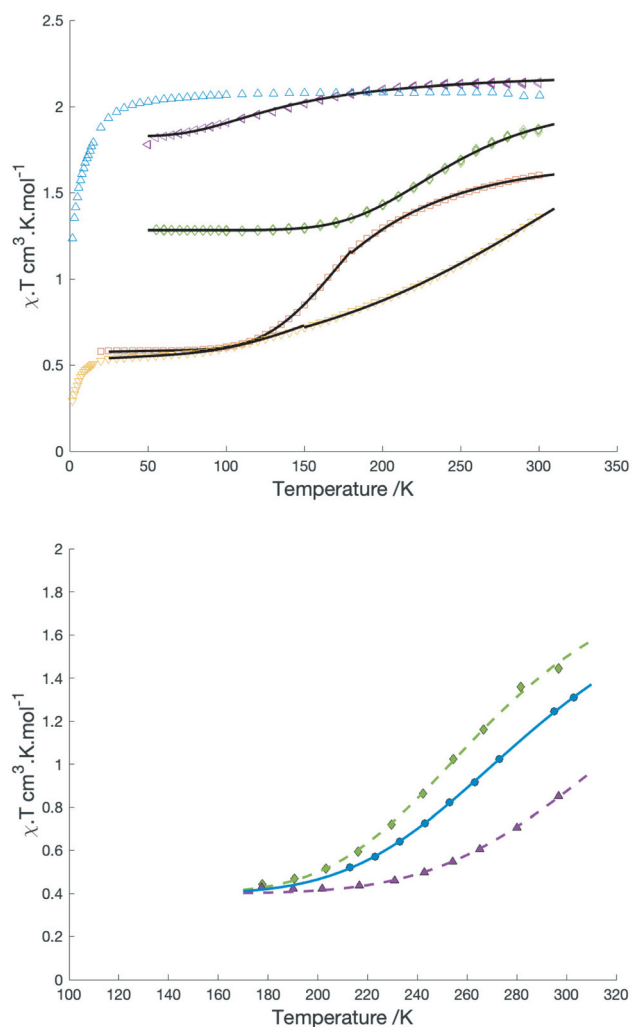


Fig. 2 Top: χT vs T for different salts of $[\text{Co}(\text{dipyvd})_2]^{2+}$: PF_6^- (blue), SbF_6^- (yellow), BF_4^- (red), OTf^- (purple), BARF_4^- (green). Black solid lines are the best fits to the simple equilibrium model described in the text. Bottom: plots of χT vs. T in solution for $[\text{Co}(\text{dipyvd})_2]^{2+}(\text{BARF}_4^-)_2$ in dichloromethane (green), $[\text{Co}(\text{dipyvd})_2]^{2+}(\text{PF}_6)_2$ in acetonitrile (blue) (data from ref. 4) and $[\text{Co}(\text{dipyvd})_2]^{2+}(\text{OTf})_2$ in dichloromethane (purple). Lines are best fits to the model in the text.

$[\text{BARF}_4^-]$ salts respectively, while the triflate transition only occurs below 150 K and does not reach a plateau above 50 K. Plots of χT vs. T for the solid samples are shown in Fig. 2.

Neither the triflate, nor the $[\text{BARF}_4^-]$ salt gave crystals amenable to X-ray analysis, so our understanding of these structures is more limited; however, X-ray quality crystals could be obtained from the PF_6^- , BF_4^- and SbF_6^- salts. The PF_6^- salt was reported previously.¹⁰ Unit cell parameters for the BF_4^- and SbF_6^- salts are reported in Table 1.

The BF_4^- salt crystallizes in the orthorhombic space group $Fddd$ with the cation centered on (and thus disordered about) the intersection of three perpendicular twofold axes. At 250 K, the verdazyl ring is essentially planar; the deviation of the verdazyl ring atoms from their mean plane is 0.03 Å. When the temperature is reduced to 150 K the deviation of the verdazyl

atoms from their mean plane increases to 0.13 Å and the average metal–ligand bond length drops from 2.019 to 1.971 Å. Between 150 K and 100 K the crystal appears to undergo a phase change and at 100 K the structure can no longer be accurately determined. These observations suggest a transition to a low spin configuration of the metal ion and electron transfer to the ligand consistent with the magnetic data, but, because of the orientational disorder of the molecules about the twofold axes of the spacegroup, they do not provide insight into the localized or delocalized structure of the low spin state.

The SbF_6^- salt crystallizes from dichloromethane/acetonitrile in the monoclinic space group $P2_1/c$. There are three anion sites; one is located on a crystallographic inversion center and thus has a site occupancy of 0.5. To compensate for this fractional occupancy one of the remaining anion sites is



Table 1 Crystallographic details for [Co(dipyvd)₂](BF₄)₂ and [Co(dipyvd)₂](SbF₆)₂

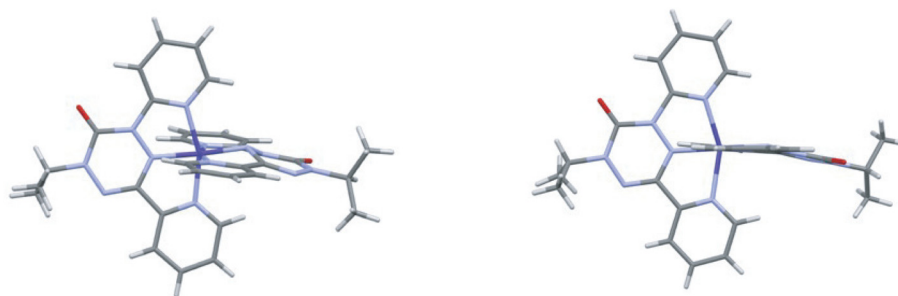
	[Co(dipyvd) ₂](BF ₄) ₂	[Co(dipyvd) ₂](BF ₄) ₂	[Co(dipyvd) ₂](SbF ₆) ₂	[Co(dipyvd) ₂](SbF ₆) ₂
CCDC deposition number	2332798	2332825	2332770	2332805
Measurement temperature/K	250	150	300	150
Crystal system	Orthorhombic	Orthorhombic	Monoclinic	Monoclinic
Space group	<i>Fddd</i>	<i>Fddd</i>	<i>P2₁/c</i>	<i>P2₁/c</i>
<i>a</i>	13.1032(8)	13.0663(16)	9.0686(7)	9.1759(10)
<i>b</i>	17.2017(10)	17.1914(18)	29.208(2)	28.242(3)
<i>c</i>	30.254(2)	29.810(7)	16.0218(12)	15.6923(16)
α	90	90	90	90
β	90	90	103.966(2)	103.842(2)
$\epsilon\epsilon$	90	90	90	90
<i>Z</i>	8	8	4	4
<i>R</i> ₁	8.44	8.44	7.76	6.36

half occupied by CH₂Cl₂ solvent. At 300 K one of the anions shows some rotational disorder, but this is no longer apparent at 150 K. The cation has two distinct ligands with no obvious orientational disorder. The two ligands have different geometries. In one ligand the central tetrazane ring is planar and the ring is relatively symmetric. For the second ligand the tetrazane ring is distinctly puckered and there is a pronounced bond length alternation consistent with an anti-aromatic 8 π electron configuration. These differences become more pronounced at 150 K. Structures of the SbF₆⁻ salt at 300 K and 150 K are shown in Fig. 3.

The (IUPAC) atomic numbering scheme for the ligand is shown in Scheme 1. Details of the coordination geometries of the metal ion, along with other structures for comparison are listed in Table 2. Similarly, selected geometrical parameters of the ligands, along with parameters from related species, are listed in Table 3.

The structure of the SbF₆⁻ salt along with the three carbonyl stretches in the IR of this species (one for the *S* = 3/2 tautomer, the other two for the distinct ligands of the *S* = 1/2 tautomer) provides strong evidence that the structure of the low spin state is localized in at least this crystal structure, but considering the small energy differences between different electronic structures and geometries in spin transition systems, it is still possible that the valence tautomer is delocalized in solution.¹⁷ A more detailed investigation of the solution IR spectra as a function of solvent helps resolve this issue. In particular since [BAR^F₄]⁻ is a very weakly-coordinating anion, solutions of this salt are expected to show minimal ion pairing effects and reflect just cation solvent interaction.

Fig. 1b shows the carbonyl region of the IR for the [BAR^F₄]⁻ salt in the solvents dichloromethane, acetonitrile, and methanol along with the triflate salt in dichloromethane. In particular for acetonitrile there are prominent maxima in the spec-

**Fig. 3** Structure of the cation in [Co(dipyvd)₂]²⁺(SbF₆)₂ at 150 K (left) and 300 K (right).**Table 2** Coordination geometries of different Cobalt species with dipyvd and terpy ligands

Substance	[Co(dipyvd) ₂](SbF ₆) ₂	[Co(dipyvd) ₂](SbF ₆) ₂	[Co(dipyvd) ₂](BF ₄) ₂	[Co(dipyvd) ₂](BF ₄) ₂	[Co(dipyvd) ₂](PF ₆) ₂ ^a	[Co(terpy) ₂](BF ₄) ₂ ^b	[Co(terpy) ₂](BF ₄) ₂ ^b
Temp./K	300	150	250	150	150	375	100
Mean Co-N distance	2.019	1.938	2.019	1.971	2.120	2.115	2.031
Σ^c	111.0	85.0	108.3	96.9	139.1	120	90.4
θ^c ^{15,16}	356.4	289.3	347.8	344.4	440.0	387	305

^a Data from ref. 4. ^b Data from ref. 24. ^c Determined using Octadist.¹⁶ Σ and θ are measures of distortion from an ideal octahedral geometry.



Table 3 Geometrical parameters for verdazyl ligands in [Co(dipyvd)₂]₂X₂ and related structures

Parameter (IUPAC numbering) – see Scheme 1	[Co(dipyvd) ₂](SbF ₆) ₂ (radical ligand)	[Co(dipyvd) ₂](SbF ₆) ₂ (anionic ligand)	[Co(dipyvd) ₂](SbF ₆) ₂ (radical ligand)	[Co(dipyvd) ₂](SbF ₆) ₂ (anionic ligand)	[Co(dipyvd) ₂](PF ₆) ^a	dipyvdH ^b
Temp./K	300	300	150	150	150	300
N4–N5	1.355(9)	1.383(9)	1.359(5)	1.415(6)	1.425(3)	1.434(3)
C3–N4	1.335(9)	1.35(1)	1.326(6)	1.375(6)	1.357(5)	1.373(3)
N2–C3	1.314(8)	1.32(1)	1.310(6)	1.309(7)	1.284(3)	1.282(3)
N1–N2	1.351(10)	1.36(1)	1.358(6)	1.377(7)	1.415(5)	1.410(3)
Planarity ^c	0.018	0.023	0.016	0.081	0.13	0.172
Sum of bond angles of coordinated atom	360.0	355.3	360.0	340.1	338.9	334.9 ^d

^a Data from ref. 4. ^b Data from ref. 24. ^c Mean distance of the verdazyl ring atoms from their own mean plane. ^d Sum of bond angles around the N–H nitrogen.

trum at 1725 and 1700 cm⁻¹ and more detailed inspection reveals a shoulder at 1740 cm⁻¹. In comparison, in dichloromethane, there is one prominent C=O stretch at 1740 cm⁻¹ and the peaks at 1725 cm⁻¹ and 1700 cm⁻¹ are reduced to inconspicuous shoulders. Since the [BAR^F₄]⁻ salt, which is largely high spin in the solid state at ambient temperature, shows only the peak at 1740 cm⁻¹ in the solid state, this is likely associated with the high spin tautomer, while the two lower frequency peaks are from the low spin species. The presence of two carbonyl stretches associated with the low spin species is consistent with a localized structure with the peak at 1725 cm⁻¹ due to the radical ligand, while that at 1700 cm⁻¹ due to the anionic ligand. Vibrational frequencies of mixed valence species can provide insight into the strength of the interaction between the two redox sites (and thus the Robin-Day classification). In particular Atwood and Geiger¹⁸ developed a charge distribution parameter for mixed valence species based on IR measurements, Δρ, defined as:

$$\Delta\rho = \frac{(\Delta\nu_{\text{ox}} - \Delta\nu_{\text{red}})}{2(\nu'_{\text{ox}} - \nu'_{\text{red}})}$$

where $\Delta\nu_{\text{ox}} = \nu'_{\text{ox}} - \nu_{\text{ox}}^{\text{means}}$, $\Delta\nu_{\text{red}} = \nu'_{\text{red}} - \nu_{\text{red}}^{\text{means}}$, and ν'_{ox} is the vibrational frequency of the system when both redox active entities are in the oxidized state; similarly ν'_{red} is vibrational frequency of the system when both redox active entities are in the reduced state. The value of Δρ varies from near zero for a completely localized, class I system, to 0.5 for a delocalized class III system. Using the carbonyl frequencies of cobalt(III) species [Co(dipyvd)₂]³⁺ (C=O at 1733 cm⁻¹) and [Co(dipyvd)₂]²⁺ (C=O at 1685 cm⁻¹)¹⁰ as ν'_{ox} and ν'_{red} respectively, and the values from the solution IR, 1725 cm⁻¹ and 1700 cm⁻¹ as $\nu_{\text{ox}}^{\text{means}}$ and $\nu_{\text{red}}^{\text{means}}$, we obtain Δρ = 0.24 indicating significant interaction between the ligands; *i.e.* a class II system. This analysis must be treated with a little caution however; unlike the related species [Ni(dipyvd)₂]²⁺ and [Zn(dipyvd)₂]²⁺ for which the C=O stretching frequencies are essentially invariant in solid and solution, the C=O stretches for [Co(dipyvd)₂]²⁺ species are quite sensitive to the molecular environment, as can be seen by comparison of the solid and solution IR spectra. Even in solution, though the [BAR^F₄]⁻ salt seems to

show the same three C=O stretching frequencies at different intensities depending on solvent, examination of the OTf⁻ spectrum indicates the C=O stretch can also depend upon counterion.

A class II Mixed valence system would be expected to show an intervalence charge transfer band; however, the overlapping spectra of the *S* = 3/2 and *S* = 1/2 tautomers make the identification of bands associated with the individual forms more complex. Inspection of the VT-vis-NIR spectra reveal that the relatively sharp peak at 617 nm gains intensity with lower temperatures and thus is associated with the low spin tautomer, while the broad feature at 560 nm loses intensity and is thus associated with the high spin tautomer. Surprisingly perhaps, the broad feature at 725 nm remains relatively unchanged with temperature. Approximate spectra for the low and high spin species can be derived by deconvolution using the concentrations determined by solution magnetic susceptibility. These are shown in Fig. 4.

As for the solution IR spectrum (above) the spectrum for the low spin tautomer can be compared with several cobalt(III) reference compounds; the terpyridine analog, [Co(terpy)₂]³⁺ along with the reduced species [Co(dipyvd)₂]²⁺ and the oxidized species [Co(dipyvd)₂]³⁺. All three reference compounds are low spin Co(III). Since [Co(terpy)₂]³⁺ is essentially transparent in the visible aside from weak d–d transitions¹⁹ the visible transitions in the two corresponding dipyvd species are almost certainly ligand or charge transfer (CT) based. For the trication, the bandshape and vibronic structure are similar to the intraligand transitions in the Ni²⁺ and Zn²⁺ analogs¹¹ and thus likely arises from a similar transition, that is, excitation into the verdazyl SOMO. The peak maximum is somewhat redshifted from the Zn²⁺ and Ni²⁺ species – this is probably due to the greater charge on the cation lowering the energy of the verdazyl SOMO. The broad absorbance in the spectrum of [Co(dipyvd)₂]²⁺ at 630 nm however likely arises from a ligand–metal charge transfer transition (LMCT) since the coordinated leucoverdazyl ligand itself only shows a tail into the visible range.¹¹ The low temperature spectrum arising from deconvolution of the VT spectra shows both the sharper intra-ligand transitions associated with a coordinated radical and a broad



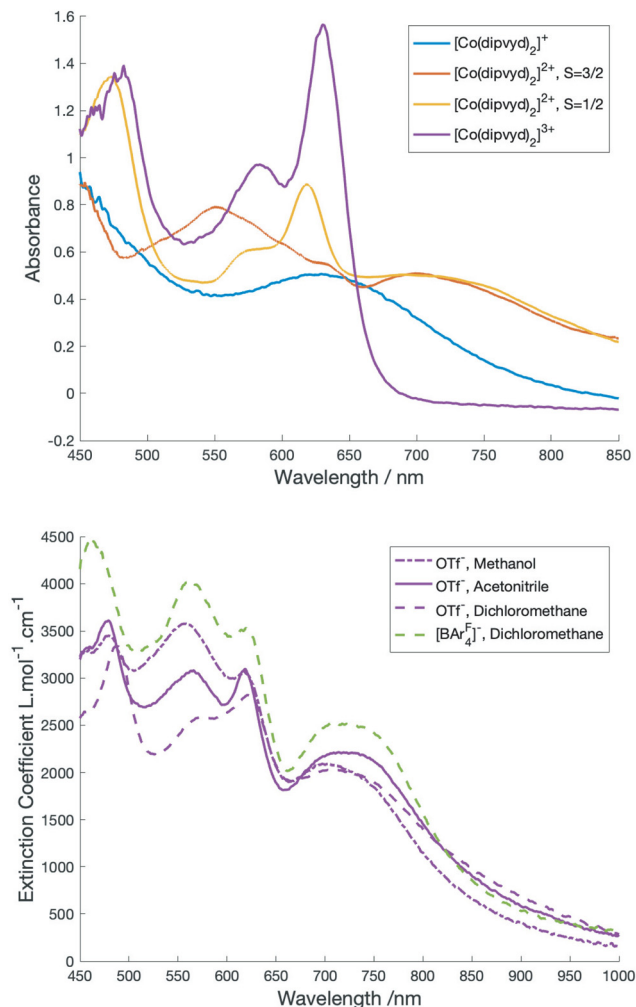


Fig. 4 Top: electronic spectra of $[\text{Co}(\text{dipyvd})_2]^{2+}$ (blue), The low spin ($S = 1/2$) and high spin ($S = 3/2$) forms of $[\text{Co}(\text{dipyvd})_2]^{2+}$ obtained by deconvolution (yellow and orange respectively), and $[\text{Co}(\text{dipyvd})_2]^{3+}$. Bottom: solvent and counterion dependence of the electronic spectrum of $[\text{Co}(\text{dipyvd})_2]^{2+}$.

band similar to the LMCT band observed for the coordinated anion. The expected intervalence charge transfer (IVCT) band probably overlaps with the LMCT band and may contribute to its asymmetric appearance.

The $S = 3/2$ state

Like the low spin state, the high spin state was incompletely characterized in our previous report. Crystallographic cobalt-ligand bond lengths and octahedral distortion parameters are comparable with other high spin octahedral cobalt species (Table 2), while the IR data and ligand geometries are consistent with radical ligands (Table 3). The problem is that traditional coupling of the radical ligands ($S = 1/2$) to the high spin cobalt ion ($S = 3/2$) would be expected to give either a sextet ($S = 5/2$, ferromagnetic coupling) or doublet ($S = 1/2$, antiferromagnetic coupling) while the high field EPR and magnetism data reported previously,¹⁰ along with magnetization

vs. field measurements at low temperature (ESI[†]) are all consistent with a spin quartet ($S = 3/2$) with significant zero field splitting ($D = +16 \text{ cm}^{-1}$). A similar phenomenon was observed in the oxolene valence tautomer $\text{Co}(3,5\text{-DBSQ})_2(\text{TMED})$, for which Pierpont *et al.* proposed that the coupling was in fact weak, and all states were roughly equally populated.²⁰ Other evidence suggests that coupling of high spin Co^{2+} to single semiquinones²¹ or verdazyl radicals²² is ferromagnetic, though as Gransbury and co-workers point out, the coupling is anisotropic with spin-orbit coupling playing a significant role, and is likely extremely dependent on subtle geometry changes.²¹ Furthermore, Robert and co-workers' computational studies on this species²³ provided the important insight that in a paramagnetic ligand field capable of two spin states, the metal ion cannot necessarily be described as purely 'low spin' or 'high spin' (a phenomenon labeled *spinmerism*). Despite this complexity we considered that a better understanding of the system might start through determination of traditional ligand field parameters and comparison with similar systems but with closed shell ligand manifolds.

Earlier studies indicate that the ligand field splittings of $[\text{Ni}(\text{dipyvd})_2]^{2+}$ and $[\text{Ni}(\text{terpy})_2]^{2+}$ are comparable.¹¹ Consequently, it is reasonable to assume that the electronic structures of $[\text{Co}(\text{dipyvd})_2]^{2+}$ and $[\text{Co}(\text{terpy})_2]^{2+}$ will show some similarity, at least with regard to the metal ion, and that $[\text{Co}(\text{terpy})_2]^{2+}$ will provide a useful point of comparison.

$[\text{Co}(\text{terpy})_2]^{2+}$ is a spin crossover compound with a high spin ($S = 3/2$) and low spin ($S = 1/2$) state in equilibrium depending upon the temperature and counterion.^{24–26} The coordination geometries of both the high spin and low spin states are detailed in Table 2. Several authors have examined the electronic structure of both the high spin and low spin states of $[\text{Co}(\text{terpy})_2]^{2+}$. In particular, Kremer and co-workers²⁴ estimated the ligand field splitting, $10Dq$, for the high spin configuration as $13\,500 \text{ cm}^{-1}$, while for the low spin configuration $10Dq$ was reported as $15\,000 \text{ cm}^{-1}$. The latter number was also reported by Krivokapic *et al.*^{25,26} As previously mentioned,¹⁰ the geometry of the high spin state of $[\text{Co}(\text{dipyvd})_2]^{2+}$ is more consistent with the geometry of the high spin rather than the low spin structure of $[\text{Co}(\text{terpy})_2]^{2+}$. However, determining other parameters that can further clarify the electronic structure is more challenging. Optical transitions that can confirm the ligand field splitting are obscured by intraligand transitions as well as the spectrum of the $S = 1/2$ tautomer. As we did for the nickel analog, we turned to X-ray spectroscopy to provide better insight. Fig. 5 shows L-edge X-ray absorption spectra (XAS) recorded on $[\text{Co}(\text{dipyvd})_2]^{2+}(\text{PF}_6^-)_2$ and $[\text{Co}(\text{dipyvd})_2]^{2+}(\text{SbF}_6^-)_2$ at 300 K as well as L edge XAS spectra of $[\text{Co}(\text{terpy})_2]^{2+}(\text{PF}_6^-)_2$ and $[\text{Co}(\text{dipyvd})_2]^{2+}(\text{PF}_6^-)$ as reference compounds.

Not surprisingly considering the magnetic data, the SbF_6^- salt shows features associated with both Co^{3+} and Co^{2+} metal centers. In fact, the major features of the spectrum can be largely reproduced by a combination of the two reference spectra. More surprising is that the spectrum of the PF_6^- salt at 300 K also shows both Co^{3+} and Co^{2+} features, despite there



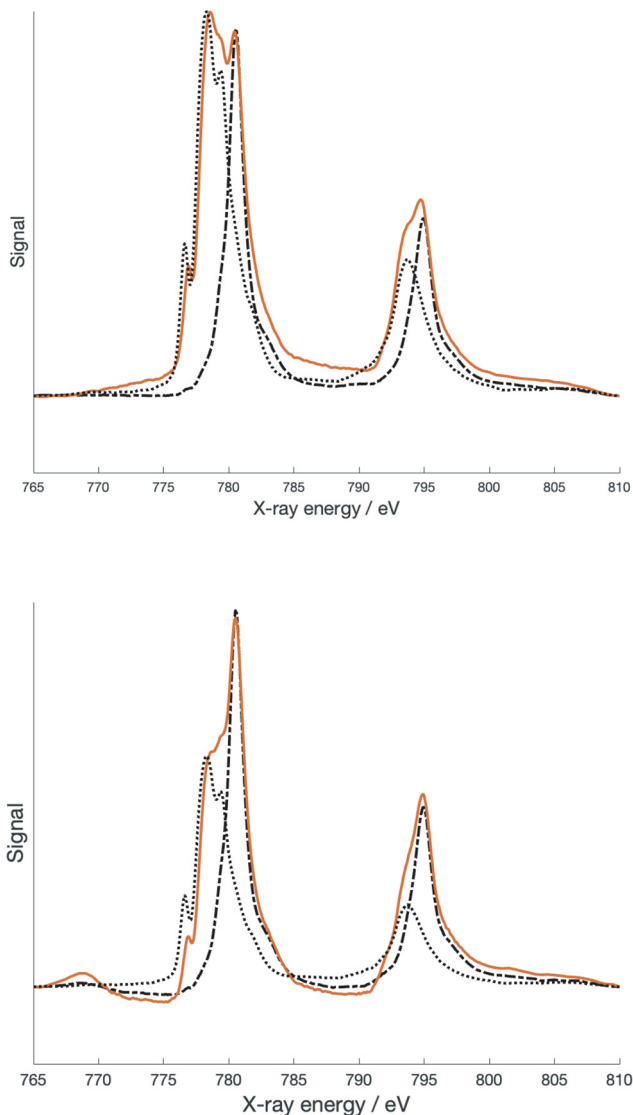


Fig. 5 XAS spectra of $[\text{Co}(\text{dipyvd})_2]^{2+}(\text{PF}_6)_2$ (top) and $[\text{Co}(\text{dipyvd})_2]^{2+}(\text{SbF}_6)_2$ (bottom) recorded at 300 K. Spectra in black are reference spectra scaled to the spectra: $\text{Co}(\text{terpy})_2(\text{PF}_6)_2$ (dotted line) and $[\text{Co}(\text{dipyvd})_2]^+$ (dashed line).

being no evidence for population of the low spin state in the PF_6^- salt at this temperature. The PF_6^- salt was further examined at 2 K by XAS and X-ray magnetic circular dichroism (XMCD). At low temperatures, the Co^{3+} features in the PF_6^- salt XAS spectrum become more prominent, though in prior studies there was no evidence for the low spin species in the low temperature EPR and magnetic data.¹⁰ There are two possible explanations for this phenomenon. The most likely results from the fact that X-ray spectroscopy is largely a surface phenomenon. At the surface of samples of $[\text{Co}(\text{dipyvd})_2]^{2+}(\text{PF}_6^-)_2$ the lattice forces that prevent relaxation of the molecules to the $S = 1/2$ state are reduced. Alternatively, this could be an example of Soft X-ray Induced Excited Spin State Trapping (SoXIESST), though this phenomenon has not been previously observed at ambient temperature.²⁷

The presence of overlapping signals complicates the simulation of the XAS spectra; however, the XMCD signal is expected to arise almost entirely from the Co^{2+} species and thus simulation of this signal may provide better insight. The XMCD data collected at 2 K is shown in Fig. 6.

Surprisingly, the best fit to the XMCD signal is obtained with $10Dq = 2.0$ eV ($16\,100\text{ cm}^{-1}$) and Slater–Condon integrals scaled by a factor of 0.69 corresponding to a Racah B parameter of 670 cm^{-1} . These parameters are more consistent with a low spin Co^{2+} center, but this is inconsistent with the geometric parameters determined at 150 K, and more crucially the EPR spectrum at 5 K.^{10,24} Several recent publications have provided evidence for low spin cobalt ions in cobalt oxolene valence tautomers.^{6–8} A quartet state can arise from ferromagnetic coupling of a low spin Co^{2+} with the two radicals, and thus our data suggests an equilibrium population of two distinct quartet states. Alternatively this could be a manifestation of the spinmerism phenomenon described by Robert *et al.*²³ Initial density functional calculations on the quartet state of $[\text{Co}(\text{dipyvd})_2]^{2+}$ using the B3LYP functional favor the low spin Co^{2+} geometry as an energy minimum, but since the results of DFT calculations on VT systems are critically dependent upon the functional used, and the calculations must also take into account intermolecular interactions,²⁸ we do not put much weight on this result; rather, we consider the complexity of this system requires a separate, dedicated computational study.

Other spectral measurements also hint at the complexity of the electronic structure of this species. Based on the analysis of the solution IR for $[\text{Co}(\text{dipyvd})_2]^{2+}[\text{BAR}^{\text{F}_4}]_2$ (above), the solvated $[\text{Co}(\text{dipyvd})_2]^{2+}$ cations exhibit a single C=O stretch at 1740 cm^{-1} . This is significantly higher than the C=O stretch in other $[\text{M}(\text{dipyvd})_2]^{2+}$ complexes (C=O at 1725 cm^{-1} , $\text{M}=\text{Fe}$,¹² Ni , Zn ¹¹) and also in $[\text{Co}(\text{dipyvd})_2]^{3+}$, (C=O at

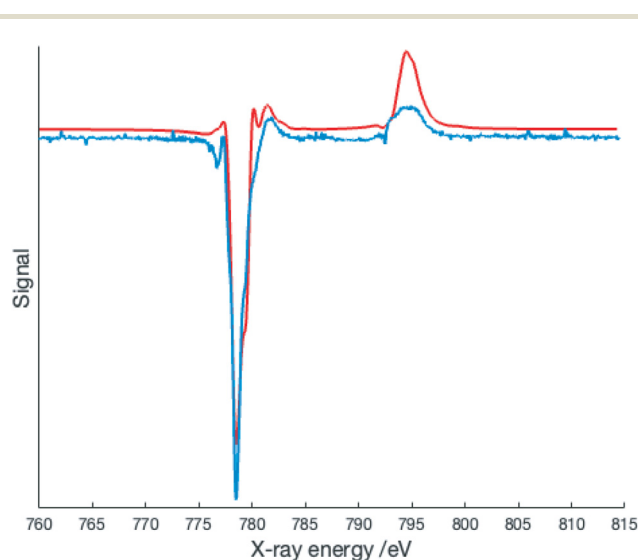


Fig. 6 XMCD spectrum of $[\text{Co}(\text{dipyvd})_2]^{2+}(\text{PF}_6)_2$ at 2 K/6T (blue) along with crystal field multiplet simulation (red line) – simulation parameters $10Dq = 2.0$ eV, Slater–Condon integrals scaled by a factor of 0.69.



1733 cm⁻¹). The 1740 cm⁻¹ stretching frequency is maintained in the solid state for the [BAR^F₄]⁻ salt, but not for the triflate or PF₆⁻ salt which both have a single C=O stretch at 1725 cm⁻¹ in line with observations for other [M(dipyvd)₂]²⁺ species. The verdazylum cations derived from oxidation of 1,5-diisopropyl verdazyls have C=O stretches in 1740 cm⁻¹ region,²⁹ suggesting that in solution, or in the environment provided by the [BAR^F₄]⁻ counterions, the high spin form of [Co(dipyvd)₂]²⁺ has some degree of *positive* charge on the verdazyl ligands. It is possible that this reflects contributions to the electronic structure of this system where the metal ion is formally *d*⁸ Co (I). Such electronic structures are still consistent with an overall spin of 3/2 and have a precedent in that the related reduced species, [Co(terpy)₂]⁺, is best described as a Co(I) system,³⁰ but more investigation is clearly necessary.

Equilibrium and environment

With (somewhat) better descriptions of the two valence tautomers, we turned to examine possible factors that influence the equilibrium between them. The solvent dependence of the C=O stretching frequency has already been noted. Solution magnetic susceptibility of the [BAR^F₄]⁻ salt in dichloromethane and acetonitrile (as determined by Evans method) is shown in Fig. 2b. Also shown is the data for the triflate salt in dichloromethane. The magnetic data was fitted to a simple equilibrium model³¹ to give estimates of ΔH and ΔS listed in Table 4.

Fig. 4b shows the vis-NIR spectra of the triflate and [BAR^F₄]⁻ salt as a function of solvent. The magnetic data, along with the IR and vis-NIR spectra all indicate that the low spin form is slightly more favored by polar solvents. This is somewhat expected from the dipole generated by localization of charge on one ligand. However, this description is simplistic. The low spin state is not exceptionally favored in methanol, even though hydrogen bonding might be expected to stabilize the development of negative charge on the carbonyl carbon. Conversely in the less polar solvent dichloromethane, the equilibrium is strongly influenced by counterion, with triflate favoring the *S* = 1/2 form. It seems likely that ion pairing plays

a big role in this behavior but at first glance the presence of negatively charged ions near the ligands would disfavor the development of a negative charge on the ligand.

The entropy associated with the VT transition is lower than that typically observed for the cobalt-oxolene valence tautomers.^{31,32} For the oxolene systems, the increase in entropy is generally attributed to increased vibrational entropy as a result of the lower force constants for the Co²⁺-ligand bonds. The lower entropy change in the present system probably reflects greater vibrational entropy associated with the more flexible geometry of the ligand in the low spin state.

The large change in ligand geometry upon tautomerization is also likely responsible for the variety of behavior observed in the solid state from entirely high spin throughout the temperature range (PF₆⁻) to mostly low spin (SbF₆⁻). In particular, the fact that in general the tautomeric transition does not go to completion at low temperature in the solid reflects the geometric requirements of the reduced ligand. Similar to the approach we used for the solution data, a simple equilibrium model can be used to fit the magnetic data in the solid state. For the [BAR^F₄]⁻ salt and triflate, this model provides acceptable fits for the entire range between 50 and 300 K. For the SbF₆⁻ and BF₄⁻ salts, such a simple model is inadequate, but reasonable fits are obtained by fitting the data in two separate temperature ranges. Values for ΔH and ΔS obtained from these fits are listed in Table 4; however, as noted by LaBute and co-workers,³³ such fits assume that valence tautomerization occurs randomly throughout the sample, whereas in practice there may be clustering of tautomers as a result of intermolecular interactions within the lattice. Consequently, the values should be treated with a little skepticism. Nevertheless, the reduction in the apparent ΔH and ΔS at higher temperatures in the BF₄⁻ salt indicates a level of cooperativity between molecules which suggests the possibility of more abrupt transitions and hysteresis with careful tuning of this or related systems.

Conclusion

More extensive studies on the [Co(dipyvd)₂]²⁺ system have provided more information on the two VT states in equilibrium. In particular, the low spin state has predominantly low spin Co³⁺ character with a localized, mixed valent ligand manifold and some degree of interaction between the ligands. The high spin state is a spin quartet, but a fully satisfactory description of its electronic structure is still elusive, with different analytical methods suggesting high spin Co²⁺, low spin Co²⁺ and even possibly Co⁺ character. The geometry changes associated with the VT transformation result in lower entropy changes compared to the more common oxolene systems, but suggest a potential for cooperative behavior in the solid state, though such behavior has not yet been realized. Together these observations suggest avenues for further study of this system, along with potential design criteria for tuning VT behavior of this and other verdazyl based coordination compounds.

Table 4 Thermodynamic parameters for valence tautomerization in salts of [Co(dipyvd)₂]²⁺

System	ΔH kJ mol ⁻¹	ΔS J K ⁻¹
[Co(dipyvd) ₂] (PF ₆) ₂ CH ₃ CN solution	18	66
[Co(dipyvd) ₂] (BAR ^F ₄) ₂ CH ₂ Cl ₂ solution	17	65
[Co(dipyvd) ₂] (OTf) ₂ CH ₂ Cl ₂ solution	19	56
[Co(dipyvd) ₂] (BAR ^F ₄) ₂	15	57
[Co(dipyvd) ₂] (BF ₄) ₂	7.9 (<170 K) 6.0 (>170 K)	40 (<170 K) 33 (>170 K)
[Co(dipyvd) ₂] (SbF ₆) ₂	4.4 (<200 K) 9.7 (>200 K)	11 (<200 K) 20 (>200 K)
[Co(dipyvd) ₂] (OTf) ₂	3.6	24



Experimental

General

DipyvdH, $[\text{Co}(\text{dipyvd})_2](\text{PF}_6)$ and $[\text{Co}(\text{dipyvd})_2](\text{PF}_6)_2$ were synthesized as reported previously.¹⁰ Other chemicals were purchased from commercial suppliers.

Low temperature X-ray absorption spectra and X-ray magnetic circular dichroism spectra were recorded at the BOREAS beamline, ALBA synchrotron, Barcelona, Spain. Additional X-ray spectra were recorded at the Stanford Synchrotron Radiation Laboratory (SSRL), Stanford, CA USA. Simulations of X-ray spectra were performed with the frontend program CRISPY³⁴ and the package QUANTY.³⁵

Spectroscopic characterization of $[\text{Co}(\text{dipyvd})_2]^{3+}$

This species was generated electrochemically in solution from $[\text{Co}(\text{dipyvd})_2](\text{PF}_6)_2$ in acetonitrile using a Pt-honeycomb working electrode and 0.1 M $\text{Bu}_4\text{N}^+\text{PF}_6^-$ supporting electrolyte. Formation of the cation was monitored by UV-vis spectroscopy. The C=O region of the IR spectrum was obtained by examination of the same solution when the oxidation was complete; a single C=O stretch was observed at 1733 cm^{-1} .

$[\text{Co}(\text{dipyvd})_2](\text{OTf})_2$

Cobalt triflate (72 mg, 0.2 mmol) and dipyvdH (118 mg, 0.4 mmol) were combined in 5 mL acetonitrile and the mixture stirred vigorously while open to the air at ambient temperature for 48 h. After this period crystallization was induced by diffusion of diethyl ether into the solution. The dark purple crystals were isolated by filtration: 121 mg, 64%, IR (ATR) 1722 cm^{-1} (C=O), 1597, 1468, 1438, 1260, 1220, 1142, 1028, 773, 706 cm^{-1} ; calcd for: $\text{C}_{32}\text{H}_{30}\text{CoF}_6\text{N}_{12}\text{O}_8\text{S}_2 \cdot 2\text{H}_2\text{O}$ C, 39.07; H, 3.48; N, 17.09. Found: C 39.01, H 3.08, N 16.53.

$[\text{Co}(\text{dipyvd})_2]\text{X}_2$

$[\text{Co}(\text{dipyvd})_2](\text{OTf})_2$ and the sodium or ammonium salt of the counterion were both dissolved in the minimum amount of methanol and the solutions combined. Distilled water was added to the resulting solution. If precipitation did not occur immediately, methanol was removed by rotary evaporation until precipitation occurred. The precipitate of the salt was removed by filtration and dried under vacuum, then recrystallized as described below.

$[\text{Co}(\text{dipyvd})_2](\text{BF}_4)_2$

$[\text{Co}(\text{dipyvd})_2](\text{OTf})_2$ (18.0 mg, 0.02 mmol) and NaBF_4 (10 mg, 0.1 mmol) gave 6.0 mg, (0.007 mmol, 36%) of $[\text{Co}(\text{dipyvd})_2](\text{BF}_4)_2$ recrystallized by vapor diffusion of ether into an acetonitrile solution. IR (ATR) 1725 (C=O), 1691 (C=O), 1603, 1595, 1481, 1463, 1437, 1276, 1247, 1217, 1157, 1051 (B-F), 1030 (B-F), 785, 630 cm^{-1} . Calcd for: $\text{C}_{30}\text{H}_{30}\text{B}_2\text{CoF}_8\text{N}_{12}\text{O}_2$: C, 43.77; H, 3.67; N, 20.42. Found: C, 43.48; H, 3.74; N 20.16. A single crystal of dimensions $0.089 \times 0.123 \times 0.584\text{ mm}$ was mounted for examination by crystallography at 150 K. A second crystal of dimensions $0.015 \times 0.204 \times 0.298\text{ mm}$ was mounted for examination by crystallography at 150 K. Unit cell

dimensions for both data collections are listed in Table 1. Full details of data collection and refinement are available from the Cambridge Crystallographic Data Centre in .cif format.

$[\text{Co}(\text{dipyvd})_2](\text{BAR}^{\text{F}}_4)_2$

$[\text{Co}(\text{dipyvd})_2](\text{OTf})_2$ 18 mg, 0.02 mmol, and $\text{NaBAR}^{\text{F}}_4$ (34 mg, 0.04 mmol) gave 20.7 mg (0.009 mmol, 44%) of $[\text{Co}(\text{dipyvd})_2](\text{BAR}^{\text{F}}_4)_2$, recrystallized by layering a dichloromethane solution with heptane and diffusion of the layers. IR (ATR) 1740 (C=O), 1606, 1464, 1440, 1353, 1274, 1110 (C-F), 887, 838, 775, 743, 711, 682, 669 cm^{-1} . Calcd for: $\text{C}_{94}\text{H}_{54}\text{B}_2\text{CoF}_{48}\text{N}_{12}\text{O}_2$: C, 47.52; H, 2.29; N, 7.07. Found: C, 47.37; H, 2.18; N 6.48.

$[\text{Co}(\text{dipyvd})_2](\text{SbF}_6)_2$

Cobalt triflate (72 mg, 0.2 mmol) and dipyvdH (118 mg, 0.4 mmol) were combined in 5 mL acetonitrile and the mixture stirred vigorously while open to the air at ambient temperature for 48 h, after which the solvent was removed by evaporation. The residue was redissolved in methanol and filtered before adding a solution of 108 mg NaSbF_6 in water to the filtrate. Methanol was removed by rotary evaporator and the resulting precipitate removed by filtration. The precipitate was redissolved in acetonitrile and crystallization induced by diffusion of dichloromethane vapor into the solution giving the product as dark green crystals. (25.9 mg, 11% from Co (OTf)₂) IR (ATR) 1725 (C=O), 1699 (C=O), 1669 (C=O), 1599, 1438, 1367, 1274, 1244, 1211, 1148, 1017, 779, 734, 659 cm^{-1} (Sb-F). Calcd for: $\text{C}_{30}\text{H}_{30}\text{CoF}_{12}\text{N}_{12}\text{O}_2\text{Sb}_2 \cdot (\text{CH}_2\text{Cl}_2)_{0.5}$: C, 31.48; H, 2.69; N, 14.45. Found: C, 31.59; H, 2.72; N 14.31. A single crystal of dimensions $0.4 \times 0.1 \times 0.1\text{ mm}$ was mounted for examination by crystallography at 300 K and 150 K. Unit cell dimensions are listed in Table 1. Full details of data collection and refinement are available from the Cambridge Crystallographic Data Centre in .cif format.

Conflicts of interest

There are no conflicts to declare.

Acknowledgements

Financial support was provided by the National Science Foundation (CHE-1900491 to DJRB). Magnetic data for $[\text{Co}(\text{dipyvd})_2](\text{BAR}^{\text{F}}_4)_2$ and $[\text{Co}(\text{dipyvd})_2](\text{OTf})_2$ were recorded on instrumentation supported by the National Science Foundation (grant MRI-1827433). Crystallographic data for $[\text{Co}(\text{dipyvd})_2](\text{SbF}_6)_2$ were recorded with instrumentation purchased with support from the US Department of Defense (grant W911NF1910520). We thank Dr Ghenadie Novitchi and CNRS-LNCMI (Grenoble, France) for collection of magnetic data on samples of $[\text{Co}(\text{dipyvd})_2](\text{BF}_4)_2$ and $[\text{Co}(\text{dipyvd})_2](\text{PF}_6)_2$. We thank Dr Jacques Pecaut (Université Grenoble Alpes) for X-ray crystallographic studies on $[\text{Co}(\text{dipyvd})_2](\text{BF}_4)_2$. Use of the Stanford Synchrotron Radiation Lightsource, SLAC



National Accelerator Laboratory, is supported by the U.S. Department of Energy, Office of Science, Office of Basic Energy Sciences under Contract No. DE-AC02-76SF00515.

References

- C. G. Pierpont, *Coord. Chem. Rev.*, 2001, **216–217**, 99–125.
- T. Tezgerevska, K. G. Alley and C. Boskovic, *Coord. Chem. Rev.*, 2014, **268**, 23–40.
- E. Evangelio and D. Ruiz-Molina, *Eur. J. Inorg. Chem.*, 2005, **2005**, 2957–2971.
- S. Klokishner, O. Reu and M. Roman, *Phys. Chem. Chem. Phys.*, 2021, **23**, 21714–21728.
- S. I. Klokishner and O. S. Reu, *Chem. Phys.*, 2003, **286**, 115–126.
- K. KC, T. Woods and L. Olshansky, *Angew. Chem., Int. Ed.*, 2023, **62**, e202311790.
- C. Metzger, R. Dolai, S. Reh, H. Kelm, M. Schmitz, B. Oelkers, M. Sawall, K. Neymeyr and H.-J. Krüger, *Chem. – Eur. J.*, 2023, **29**, e202300091.
- M. Mörtel, S. J. Goodner, J. Oswald, A. Scheurer, T. Drewello and M. M. Khusniyarov, *Dalton Trans.*, 2024, **53**, 4098–4107.
- M. A. Hay, J. T. Janetzki, V. J. Kumar, R. W. Gable, R. Clérac, A. A. Starikova, P. J. Low and C. Boskovic, *Inorg. Chem.*, 2022, **61**, 17609–17622.
- C. Fleming, D. Chung, S. Ponce, D. J. R. Brook, J. DaRos, R. Das, A. Ozarowski and S. A. Stoian, *Chem. Commun.*, 2020, **56**, 4400.
- C. Fleming, S. Vu, D. J. R. Brook, S. Agrestini, E. Pellegrin and J. DaRos, *Front. Chem.*, 2023, **11**, DOI: [10.3389/fchem.2023.1295289](https://doi.org/10.3389/fchem.2023.1295289).
- D. J. R. Brook, C. Fleming, D. Chung, C. Richardson, S. Ponce, R. Das, H. Srikanth, R. Heindl and B. C. Noll, *Dalton Trans.*, 2018, **47**, 6351–6360.
- S. D. J. McKinnon, B. O. Patrick, A. B. P. Lever and R. G. Hicks, *Chem. Commun.*, 2010, **46**, 773–775.
- D. J. R. Brook, *Comments Inorg. Chem.*, 2015, **35**, 1–17.
- M. Marchivie, P. Guionneau, J.-F. Letard and D. Chasseau, *Acta Crystallogr., Sect. B: Struct. Sci.*, 2005, **61**, 25–28.
- R. Ketkaew, Y. Tantirungrotechai, P. Harding, G. Chastanet, P. Guionneau, M. Marchivie and D. J. Harding, *Dalton Trans.*, 2021, **50**, 1086–1096.
- M. Parthey and M. Kaupp, *Chem. Soc. Rev.*, 2014, **43**, 5067–5088.
- C. G. Atwood and W. E. Geiger, *J. Am. Chem. Soc.*, 2000, **122**, 5477–5485.
- J. T. Yarranton and J. K. McCusker, *J. Am. Chem. Soc.*, 2022, **144**, 12488–12500.
- H. W. Liang, T. Kroll, D. Nordlund, T.-C. Weng, D. Sokaras, C. G. Pierpont and K. J. Gaffney, *Inorg. Chem.*, 2017, **56**, 737–747.
- G. K. Gransbury, M.-E. Boulon, R. A. Mole, R. W. Gable, B. Moubaraki, K. S. Murray, L. Sorace, A. Soncini and C. Boskovic, *Chem. Sci.*, 2019, **10**, 8855–8871.
- T. M. Barclay, R. G. Hicks, M. T. Lemaire, L. K. Thompson and Z. Q. Xu, *Chem. Commun.*, 2002, 1688–1689.
- P. Roseiro, N. B. Amor and V. Robert, *ChemPhysChem*, 2022, **23**, e202100801.
- S. Kremer, W. Henke and D. Reinen, *Inorg. Chem.*, 1982, **21**, 3013–3022.
- I. Krivokapic, M. Zerara, M. L. Daku, A. Vargas, C. Enachescu, C. Ambrus, P. Tregenna-Piggott, N. Amstutz, E. Krausz and A. Hauser, *Coord. Chem. Rev.*, 2007, **251**, 364–378.
- C. Enachescu, I. Krivokapic, M. Zerara, J. A. Real, N. Amstutz and A. Hauser, *Inorg. Chim. Acta*, 2007, **360**, 3945–3950.
- G. Poneti, M. Mannini, L. Sorace, P. Sainctavit, M.-A. Arrio, E. Otero, J. Criginski Cezar and A. Dei, *Angew. Chem., Int. Ed.*, 2010, **49**, 1954–1957.
- G. K. Gransbury, M.-E. Boulon, S. Petrie, R. W. Gable, R. J. Mulder, L. Sorace, R. Stranger and C. Boskovic, *Inorg. Chem.*, 2019, **58**, 4230–4243.
- B. C. Haller, D. Chambers, R. Cheng, V. Chemistruck, T. F. Hom, Z. Li, J. Nguyen, A. Ichimura and D. J. R. Brook, *J. Phys. Chem. A*, 2015, **119**, 10750–10760.
- J. England, E. Bill, T. Weyhermüller, F. Neese, M. Atanasov and K. Wieghardt, *Inorg. Chem.*, 2015, **54**, 12002–12018.
- D. M. Adams and D. N. Hendrickson, *J. Am. Chem. Soc.*, 1996, **118**, 11515–11528.
- C. G. Pierpont and O. S. Jung, *Inorg. Chem.*, 1995, **34**, 4281–4283.
- M. X. LaBute, R. V. Kulkarni, R. G. Endres and D. L. Cox, *J. Chem. Phys.*, 2002, **116**, 3681–3689.
- M. Retegan, *Crispy: v0.7.4*, 2019.
- M. W. Haverkort, M. Zwierzycki and O. K. Andersen, *Phys. Rev. B: Condens. Matter Mater. Phys.*, 2012, **85**, 165113.

